Spatially Correlated Flickering of All-inorganic Perovskite Microcrystals

*Sasank Pattnaik, Shruti Singh and Arindam Chowdhury**

Department of chemistry, Indian Institute of Technology Bombay, Powai, Mumbai-400076, India

* Email: arindam@chem.iitb.ac.in

Abstract

All-inorganic halide perovskites, especially $CsPbBr_3$ microcrystals, are often considered to be optically stable and less defect-prone compared to their organometallic counterparts. Nevertheless, reports of photoluminescence (PL) blinking in bulk perovskite systems till date are restricted to organometallic halide perovskite nano-/microrods, leaving it an open question whether similar intermittency behaviour can be observed in all-inorganic halide perovskites of comparable dimensions. Intriguingly, we witnessed multi-level PL fluctuations (*flickering*) in individual green-emitting $CsPbBr_3$ microrods. Wide-field PL microscopy reveals that the intensity fluctuations are nearly identical along the microrod, owing to charge carrier migration, and waveguide-assisted propagation. Our measurements on single microrod suggests that the flickering dynamics is strongly influenced by excitation power, excitation energy, and local environmental constituents. Under dry argon environment, a sharp reduction in the PL intensity is observed, indicating the formation of large number of nonradiative (NR) centers which quenches all the photogenerated carriers, suppressing overall emission intensity and PL flickering. The exposure of oxygen passivates these NR traps generated under argon, while humidity introduces metastable photoinduced NR traps ("*special quenchers*") that govern the enhanced flickering behaviours. Our findings establish that spatiotemporally correlated intermittency is not limited to organometallic perovskites but extends to all-inorganic perovskite bulk emitters as well and provides new insights into the role of transient defects and atmospheric constituents in dictating emission stability.

1. Introduction

Halide Perovskites have emerged as a revolutionary group of semiconductor materials for optoelectronic applications[1–5]. The high photoluminescence quantum yield, strong absorption, long carrier recombination lifetime and diffusion lengths of halide perovskite render them suitable for high-performance solar photovoltaics, light-emitting diodes (LEDs), lasers, and photodetectors[6–8]. In addition to device-level performance, the intrinsic photophysics of halide perovskites consistently reveals phenomena that challenge the established paradigms in semiconductor science. One such phenomenon is photoluminescence intermittency (or PL blinking), where the emission intensity of crystals stochastically fluctuates between multiple bright and dark states in a seemingly random yet discrete manner [9]. PL blinking has long been considered as a signature trait of quantum-confined systems like single molecules, fluorescent proteins, and semiconductor quantum dots/nanocrystals (QDs/NCs)[10,11]. In case of semiconductor QDs/NCs, the mechanism underlying the PL blinking is often associated with charging-discharging of the core or trapping of the charge carriers for extended durations within dark states (low quantum yield) formed by the high density of surface defects in the nanostructures[12,13].

PL intermittency has been reported in dimensionally unconfined (bulk, of the order of few microns), spatially extended systems, confined in 1- or 2-dimensions, where the blinking patterns were (spatially) heterogeneous and temporally uncorrelated due to the ensemble-averaging effects [14–16]. Over the last few years, organometallic halide perovskites (OHPs) including $MAPbBr_3$ and $MAPbI_3$ have shown to exhibit considerable PL intermittency,[17–19] owing to their long-range carrier diffusion lengths. More recent studies report micron-sized OHP crystals (extending beyond the optical diffraction limit) undergo blinking or flickering synchronously, with intensity changes well correlated throughout distal regions separated by several hundreds of nanometer [12,17,20]. Since these processes can adversely affect the device performance, there lies a strong interest in identifying the factors that govern PL intermittency in perovskite materials.

One of the proposed explanations for the blinking observed in entire $MAPbI_3$ single-crystal nanorods is associated with the presence of metastable nonradiative trap(s), which can effectively funnel the charge carriers through a non-radiative channel[21]. Moreover, the blinking of micron-sized $MAPbI_3$ single-crystal rods has also been ascribed to highly efficient transient non-radiative pathway(s)[17], possibly arising from the redistribution of mobile, charged (ionic)

species upon photoexcitation, which leads to the formation of massive PL in OHP crystals. This led to the introduction of the concept of '*special traps*' wherein a very few of such traps (metastable quenchers) can abruptly modulate the radiative recombination efficiency in OHP crystals over extended spatial domains[22]. Despite these insights, it remains unclear whether this mechanism alone accounts for spatially synchronous PL intermittency in micrometer-scale OHP crystals. For instance, heterogeneously distributed photoactive traps have been invoked to explain the spatially correlated PL intermittency of $MAPbI_3$ rods of length 1–2 μm [23]. Likewise, the spatiotemporally (un)correlated emissivity fluctuations of $MAPbBr_3$ microrods has been attributed to the presence of quencher(s) of varying effective quenching capabilities [24].

Despite these insights, the exact nature of metastable quenchers and the specific role of organic cations (MA^+, FA^+) remain elusive. In parallel, several studies have demonstrated that environmental species *e.g.,* oxygen, moisture, and residual gases can reversibly alter PL intensity and stability in perovskites by passivating or activating trap states, inducing photo-doping, or modifying surface chemistry [9,22,25,26]. Furthermore, environmental constituents such as oxygen, nitrogen, and moisture strongly influence intermittency[22,25,26]. Oxygen has been shown to passivate traps and enhance PL, while nitrogen can activate highly efficient nonradiative centers, leading to quenching or altered blinking dynamics[22]. Moisture, depending on relative humidity (RH), can either stabilize emission or accelerate degradation of perovskite crystals[22,25]. The observations raise a fundamental question as to whether PL blinking in OHP crystals is intrinsically linked to the presence of organic cations and their environmental sensitivity, or whether it represents a more universal phenomenon of halide perovskites. In this context, it remains unclear whether fully inorganic perovskites (*e.g.,* $CsPbX_3$), which are generally considered to be more stable and less defect-prone, also exhibit comparable spatiotemporally (a)synchronous PL fluctuations or such phenomena are restricted specifically to OHP compositions or morphologies[21]. Indeed, prior reports often show the absence of blinking in $CsPbBr_3$ microcrystals compared to their organic counterparts[27].

In a quest to explore the fundamental nature of emission dynamics in micron-sized all-inorganic halide perovskite system, we investigated PL fluctuations in individual $CsPbBr_3$ microrod (MRs). Surprisingly, in contrast to the earlier reported emission stability[27,28], we found multi-level spatiotemporally correlated PL intensity fluctuations in $CsPbBr_3$ MRs of lengths upto a few microns. Herein, we validate the transitions between *bright*- and *dim*- (and/or *gray*-) states switching frequency of the flickering events, whereas the spatial

synchronicity across the entire MR is quantified using correlation analysis of PL intensity trajectories. Further, we show the time trajectories of individual $CsPbBr_3$ MRs under sequential change of constituent atmospheric environments, correlating the temporal dynamics of non-radiative channels and atmospheric conditions. Our findings not only broaden the understanding of PL blinking beyond organometallic halide perovskite systems but also highlight the role of photo-induced defects under different local atmosphere.

2. Materials and Methods

2.1 Materials

All chemical reagents for the synthesis of $CsPbBr_3$ microcrystals, including caesium bromide (CsBr, Sigma-Aldrich, >99.9%), lead (II) bromide ($PbBr_2$, Loba Chemie Pvt. Ltd, >99.9%), N,N-dimethylformamide (C_3H_7NO, DMF, >99%), and isopropanol (C_3H_8O, IPA, >99%), were procured from Spectrochem. Pvt. Ltd. Furthermore, all chemical reagents used are of spectroscopic grade and were used as received without further purification.

2.2 Synthesis of $CsPbBr_3$ Microcrystals

$CsPbBr_3$ microcrystals were synthesized following the gas–liquid transfer recrystallization method as reported by Jiang et al. [29] Specifically, 0.0212 g (0.1 mmol) of CsBr and 0.0367 g (0.1 mmol) of $PbBr_2$ were dissolved in 2 mL of DMF and sonicated for 15-20 minutes. Subsequently, 3 µL of this solution was deposited onto a glass coverslip and allowed to crystallize in a sealed environment saturated with isopropanol vapour for 36 hours. The synthesized $CsPbBr_3$ microcrystals grown on the glass coverslip were used for further experiments.

2.3 Characterization Techniques

The microstructure morphology of the as-synthesized $CsPbBr_3$ rods on glass-coverslips were examined under field emission scanning electron microscope (FESEM, JEOL JSM-7600F). Because of the high sensitivity of the sample towards the electron beam, a 3 nm thick layer of gold (Au) was sputtered to minimize the charging effects. Further, the surface topography was explored with atomic force microscopy (AFM, Asylum Research MFP 3D). For AFM measurements, a AC-240TS tip was used in AC-mode (tapping mode) at 70 kHz drive frequency. Powder X-ray diffraction (pXRD) analysis was performed for the identification of crystal phases of the MRs on an X-ray diffractometer (Smart Lab), equipped with Cu-Kα source (wavelength ~ 1.54 Å). The solid-state UV–visible absorption spectra were collected between

480 and 500 nm by using Agilent Cary-5000 spectrophotometer, whereas the PL spectra range was collected by using Horiba Fluoromax Plus spectrofluorometer. The fluorescence lifetime imaging measurements were performed using Olympus IX73 microscope equipped with Picoquant MicroTime 200. All the PL lifetime imaging experiments were carried out using a 405 nm pulsed-laser, operating at 2 MHz repetition rate analysed with SymphoTime software. The average lifetime of the MRs were calculated by tri-exponential fitting of PL decay curves. The intensity and average lifetime traces were acquired from the photon streams binned for 50 ms.

2.4 Single-Particle PL microscopy

Spatially resolved PL measurements of the freshly grown MRs were performed using a home-built wide-field epifluorescence microscopy setup. A 405 nm (Laserglow) continuous wave laser (power density ~100 mW cm^{-2}) was used to illuminate the spatially segregated MRs using an oil immersion objective lens (1.49 NA, 60×, Nikon ApoTIRF, oil). For point excitation microscopy, we passed the collimated beam directly to the back focal plane of the oil objective. The details of optical arrangements can be found in the earlier report[30]. The emanated PL was collected through the same objective lens followed by 458 nm long-pass filter and detected using a sCMOS camera (Hamamatsu Orca flash 4.0 v3). The spatially-resolved PL spectra of individual MRs were collected using a variable slit and a 70 grooves/mm transmission grating, placed in the emission path. The detailed description of the experimental setup can be found elsewhere [31]. PL movies (16-bit images, 1×1 binning) of all MRs were collected at 50 Hz acquisition rate. PL fluctuation dynamics of $CsPbBr_3$ MRs were monitored under strategically varied dry and humid (RH ~ 50%) conditions of Argon (Ar) and Oxygen (O_2), in addition to ambience (Air) environment. A glass chamber with humidity sensor, containing an inlet and outlet, was attached to the microscope stage to attain the desired local atmospheric conditions. For 0% RH conditions, dry gases (Ar or O_2) were purged directly into the chamber, while the moist conditions were attained by purging the gases through water. The gases (dry/moist) were purged for 30 min before each measurement, without exposing the MRs to light. All the microscopy data were collected using μ-manager software at 295 K. The PL movies were analyzed using ImageJ (NIH),[32] Origin, and MATLAB (R2023a) software.

3. Results and Discussion

3.1 Structural and Optical Characterizations

The structural and optical characterizations of the synthesized $CsPbBr_3$ microcrystals are depicted in the **Figure 1**. The characteristic diffraction pattern in the pXRD spectra (**Figure 1a**) matches well with the orthorhombic phase of $CsPbBr_3$ crystals with ICSD 98-009-7851[33]. The morphological features in FE-SEM imaging reveal the formation of well separated microrods of lengths spanning from ~500 nm to several microns and widths in the range of few hundreds of nanometer (**Figure 1b**). A representative MR of length ~2 μm is shown in the inset of **Figure 1b**. Further, the AFM imaging depicts a uniform height of ~80 nm along the length of a typical MR (**Figure 1c**). These findings collectively indicate the bulk crystalline nature of the synthesized MRs.

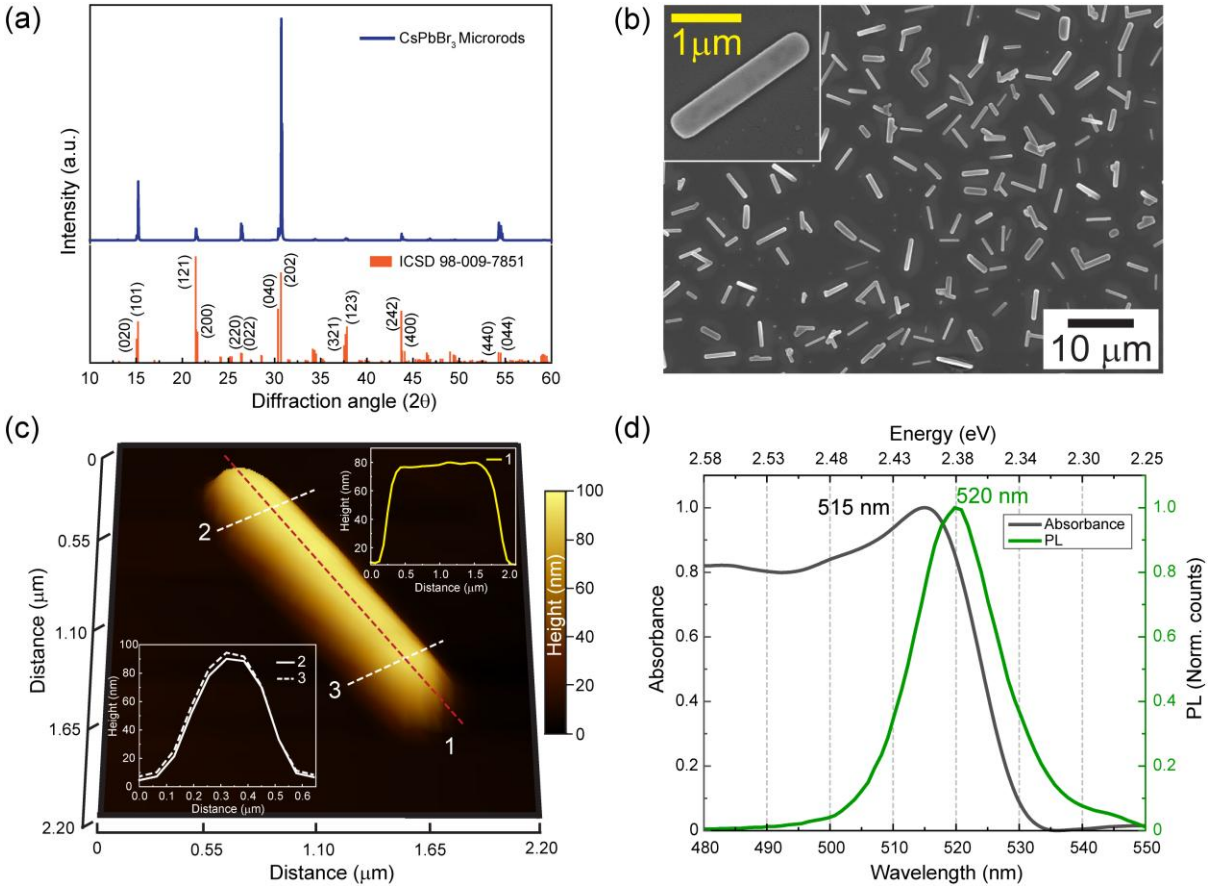

Figure 1: Structural and optical characterization of $CsPbBr_3$ MRs. (a) pXRD spectra of the MRs. (b) SEM image of as-synthesized MRs. Zoomed-in SEM image of a representative MR (inset). (c) AFM topographical image of a typical MR. Line profiles along the major and minor axes of the MR showing uniform cross-sections (insets). (d) Bulk absorption and emission spectra of $CsPbBr_3$ MRs recorded in solid-state mode.

The absorption and PL spectrum (**Figure 1d**) of the MRs in solid state show a clear excitonic absorption feature at ~515 nm (2.40 eV) and a nominal stoke shifted intense PL emission

spectrum centered at ~520 nm (2.38 eV) with a line width of 76 meV. Similar results have also been reported for other bulk structures of $CsPbBr_3$ [34,35], which suggest that excitons/carriers are not quantum-confined in any dimension, as expected from their morphology.

3.2 Evidence of PL fluctuations in $CsPbBr_3$ MRs

The spatiotemporal PL dynamics of the $CsPbBr_3$ MRs were studied under ambient conditions (~300 K, 50% RH) using epifluorescence video microscopy at 50 Hz. Following the 405 nm laser excitation, the spatially segregated crystals were identified and their PL emission was collected in an sCMOS camera. To minimize photo-induced effects such as photo-curing and degradation, the laser power density was carefully maintained at ~0.1 W/cm² during the data acquisition.

Figure 2a illustrates the representative fluorescence imaging of $CsPbBr_3$ MRs (MR-1 and MR-2), which exhibit non-uniform emission intensities across individual crystals. The contrast in the intensity likely arises from the variation in structural morphology, which in turn impact their radiative recombination dynamics. As shown in **Figure 2b,** the PL trajectories unveil abrupt jumps between multiple *bright* and *dim* (or *gray*) states on top of a slow time-varying base intensity. Here, we have considered the emission intensity of a polystyrene bead excited under 405 nm, as the base intensity. The cross-correlation values obtained from the time-resolved PL intensity traces of respective MRs {**Figure S1**, supporting information (SI)} suggest that the fluctuations found in individual MRs are distinct and heterogeneous (**See Movie-1**, SI) omitting the influence of external factors such as laser power variation or focus drifts. **Figure 2c** displays the time-averaged PL image of a representative $CsPbBr_3$ microrod (MR-3) of length ~2.5 μm. The intensity line profiles shown in **Figure 2c**(i) reveal the width ($FWHM_{1 \text{ and } 2}$ ~430 nm) of the MR-3 is beyond the optical resolution limit (diffraction-limit ~ 200 nm). This observation is in line with the SEM analysis, which confirms the lateral widths of the MRs to be around few to several hundreds of nanometers. **Figure 2c**(ii) depicts a PL intensity gradient along the length of MR-3 and enhanced intensity at the edges compared to the interiors, owing to the waveguiding nature of the self-assembled $CsPbBr_3$ MR. [36–38] Interestingly, we noticed an optical instability in entire MR-3 during the course of data acquisition, as exemplified in the time-lapse PL snapshots of MR-3 (**Figure 2d**). Similar behaviors were consistently observed for a vast majority of MRs of comparable dimensions, independent of their synthesis batch (**Figure S3**, SI).

To better understand the emission dynamics of $CsPbBr_3$ microrods, we extracted the spatially integrated PL trajectory of MR-3 for a time duration of 60 s. The intensity fluctuations were observed to occur on top of a slow varying baseline intensity indicating that the microrod never turns non-emissive. The trajectory of entire MR-3 (**Figure 2e**) reveals that the emission switches between *bright* and *dim* levels, encompassing multiple intermediate grey states, a phenomenon commonly referred to as "*flickering*". Transitions between these states typically occur over hundreds of milliseconds, with abrupt changes being less common. The 2 s temporal blow-ups (**Figure 2e** i-iv) provide evidence of such rare, high frequency jumps between two intermediate states, which take place within a few frames (20 – 40 ms).

Further, the recurrence of high frequency (> 25 Hz) PL fluctuations is validated using intensity jump distributions for MR-1, MR-2 and MR-3 (**Figure 2f**). The significantly larger width of these distributions compared to that for the background noise demonstrates that the fluctuations are intrinsic to the microrods and not experimental artefacts. We designate abrupt (40 ms) intensity jumps with amplitudes more than 3 times the standard deviation of the background fluctuations as flickering. These abrupt PL fluctuations are quantified by switching frequency (SF), defined as the number of PL intensity jump events occurring in one or two frames (20 or 40 ms) per second which exceeds a predefined threshold (**Figure S2**, SI). Additional emission trajectories for other measured MRs reflecting similar traits are shown in **Figure S3**, SI.

In contrast to, conventional two-state intermittency observed in single-quantum emitters,[10,39] the fluctuation characteristics exhibited by these all-inorganic halide perovskites closely resembles to PL fluctuations previously reported for $MAPbI_3$ microrods/discs and $MAPbBr_3$ microrods[19,21,27]. Moreover, the PL emission spectra remained unaffected throughout the measurements, suggesting that spectral diffusion is not responsible for the observed intensity fluctuations (data not shown). We further note that the PL fluctuations do not originate from localized nanodomains within individual MRs, indicative of spatially homogenous blinking dynamics across entire crystal (See **Movie-2**, SI).

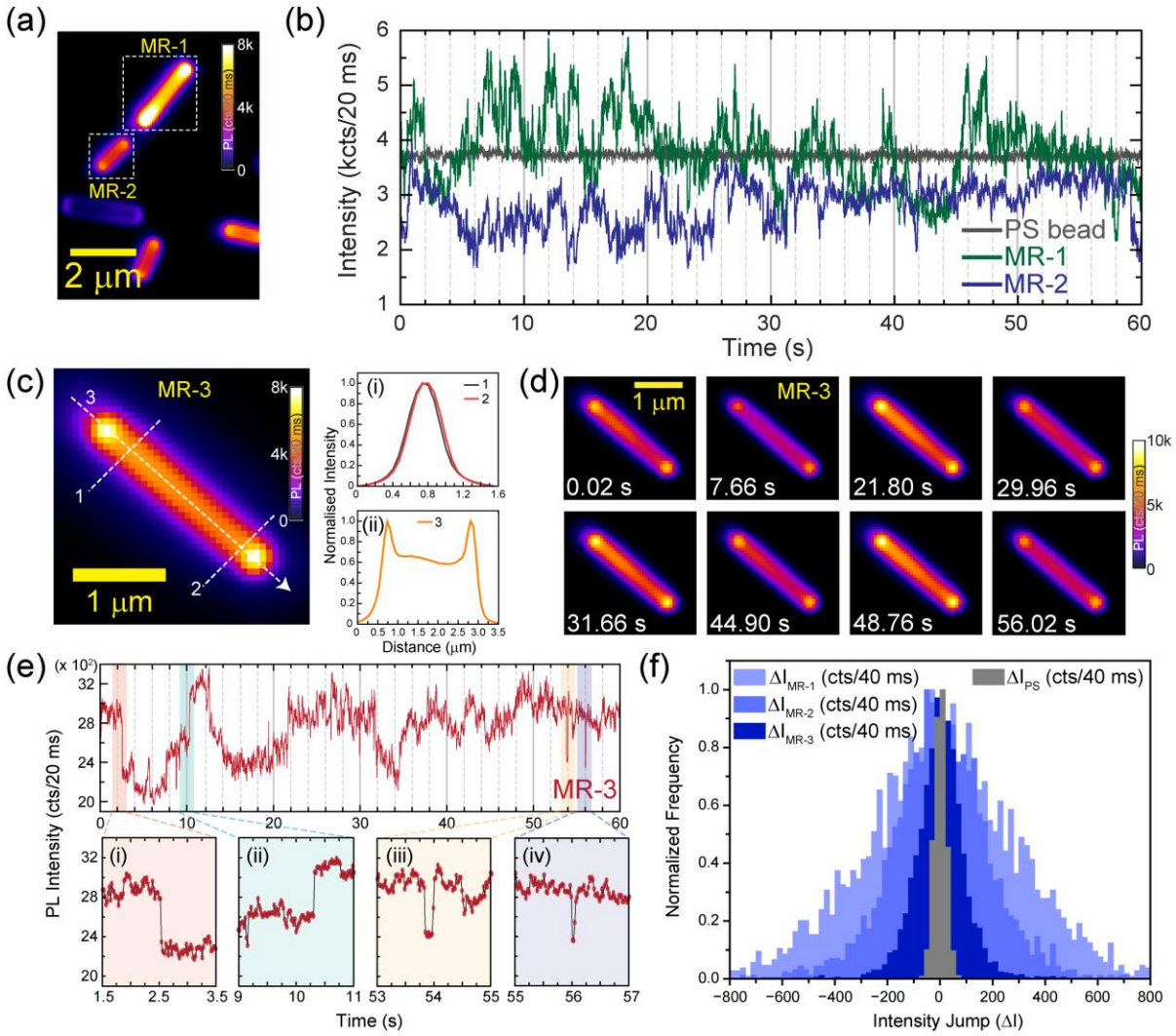

Figure 2. PL fluctuations in an individual MR. (a) PL image of *CsPbBr₃* MRs grown on a glass coverslip. (b) PL intensity trajectories of entire MR-1 and MR-2 along with that for the background noise (polystyrene bead) (c) False colour average PL image of MR-3 (length ~2.5 μm) under wide-field excitation. (i-ii) Intensity line profiles along the dashed line showing intensity gradient along the minor and major axes of MR-3. (d) Time-lapse PL snapshots of MR-3 illustrating flickering propagation. (e) Spatially integrated intensity trajectories of MR-3 showing multi-state PL fluctuations. Zoomed-in trajectories (2 s) exemplify few abrupt intensity jumps. (f) Distribution of emission intensity jumps (ΔI) values at 40 ms of MR-1, MR-2 and MR-3 along with that of PS background.

3.3 Spatial Correlation of PL Flickering in Microrods

To probe the extent of spatial homogeneity within the MRs, we analysed the PL trajectories from three distinct local domains (*I*, *II* and *III*) of MR-4 (**Figure 3a**), each separated by a distance exceeding the optical diffraction limit. The normalised average PL trace of entire MR-4 plotted along with that of nanodomains *I-III* in **Figure 3b**, reflect several abrupt transitions between *bright* and *gray* states. We observed that all the flickering events were not only identical amongst the nanodomains *I*, *II*, and *III*, but also exhibit strong temporal overlap with entire MR-4, indicating spatially concerted flickering across the microrod. A slight

variation in the amplitudes of intensity jumps was noticed, despite of the highly correlated flickering events (marked by arrowheads in **Figure 3b**). Spatiotemporal correlation across the entire MR was examined using a kymogram by sequentially stacking the intensity profile of a one-pixel strip along the major-axis of MR-4 (marked in **Figure 3a**) over the 60 s duration. The kymogram of exemplary 4 s time-windows (0 – 4 s, 23.24 – 27.22 s and 35.64 – 39.62 s) display that the entire MR-4 indeed exhibits spatially correlated flickering behaviour across the entire MR (**Figure 3c**). The Kymogram illustrating the correlated flickering along the length of MR-4 over the 60 s duration is depicted in **Figure S4,** SI. The contrasts in PL intensity along the temporal axis is a result of multi-state flickering events, whereas the uniform emission along the spatial axis highlights the in-sync change of emission states along the long axis of MR-4.

The extent of spatial correlation of PL fluctuations within the microrods was quantitatively assessed by calculating Pearson Correlation coefficients (PCC) between the PL trajectories of the nanodomains (*I*, *II*, and *III*) within MR-4. The resultant scatter plot of PL intensities presented in **Figure 3d** yields an extremely high PCC value ($r_{I\text{-}II} = 0.979$; $r_{I\text{-}III} = 0.978$), which indicates the intensity fluctuations at these distal domains (~500 nm apart) are highly synchronous. Similar analyses performed on other microrods, including MR-9 and MR-10 produced comparable results, although PCC values tend to decrease slightly with increasing spatial separation (**Figure S5-S6,** SI). Notably, $r_{I\text{-}II}$ (and $r_{II\text{-}III} = 0.991$) is marginally higher than $r_{I\text{-}III}$, suggesting a potential spatial dependence in the correlation of blinking events along the microrod. Subsequently, to probe the distance dependence of spatially concerted flickering propensity, we computed the PCC values for the time series of every pair of pixels along the major axis of the microrod. **Figure 3e** displays the generated correlation coefficient matrix ($[r_{ij}]$) for MR-4, derived from a one-pixel wide, 30-pixel-long (2 μm) strip along the rod (**Figure 3a**, dashed rectangle). In this matrix, the off-diagonal elements represent the spatial correlation of blinking (r_{ij}) between the i^{th} and j^{th} pixels. We found that r_{ij} values are uniformly high (~>0.9, mean ≈ 0.96) across the entire length of MR-4, and the weak distance dependence observed up to ~2 μm indicates that the PL flickering occurs in a highly coordinated manner across the entire crystal. These results demonstrate that the entire microrod behaves as a single, spatially coherent entity with respect to its flickering dynamics. These results are consistent with earlier reports on $MAPbBr_3$ microcrystals, where they observed synchronous blinking across entire crystal due to carrier migration and transient nonradiative traps[20,27].

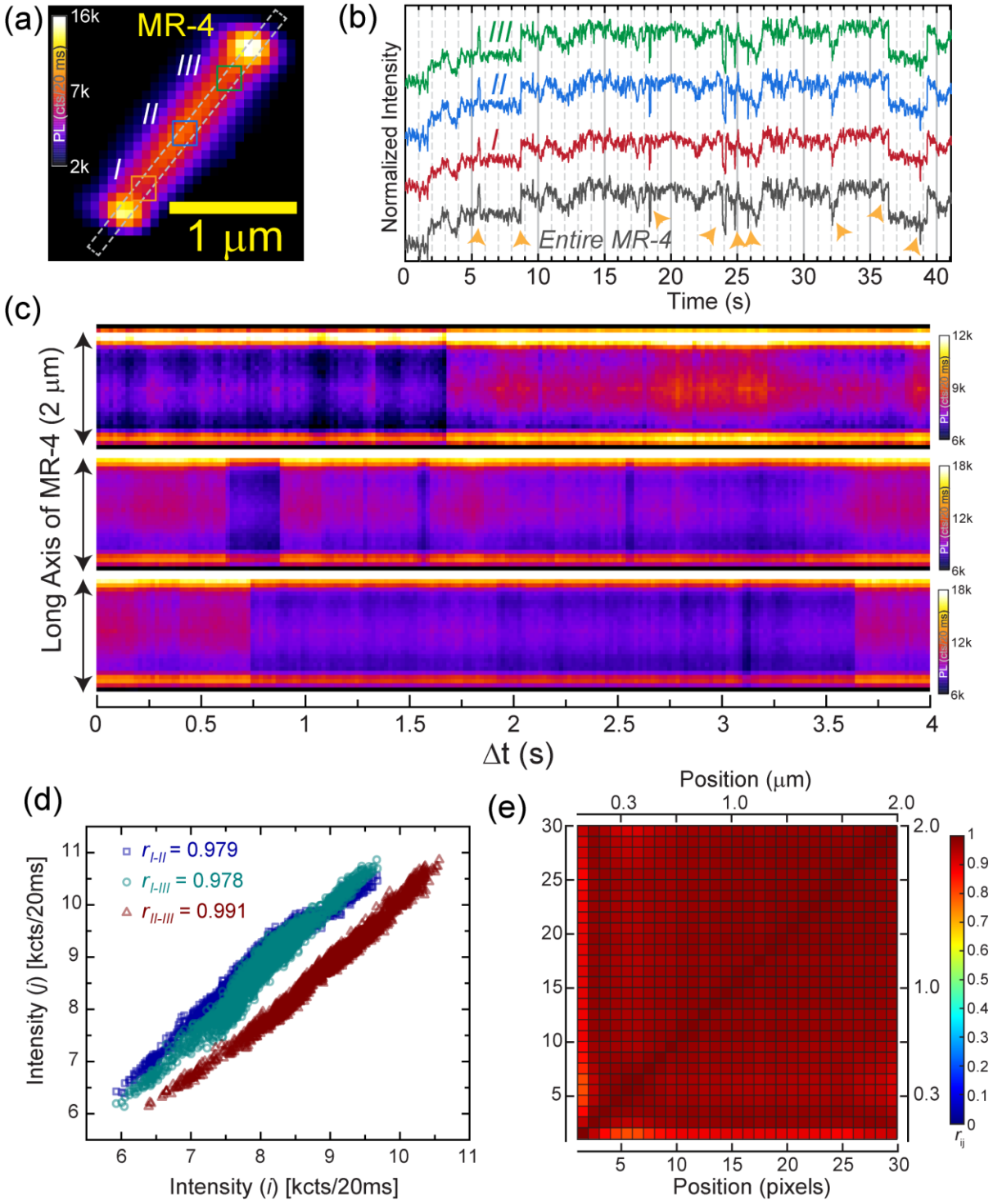

Figure 3. Spatially synchronous PL fluctuations of entire MR-4. (a) PL image of an isolated MR-4. (b) Normalized PL intensity fluctuations from three distinct domains (*I*, *II*, *III*) marked in (a), along with the PL trace of entire MR-4, shows near identical fluctuations. (c) Spatially-resolved intensity trajectory (kymogram) of MR-4, depicting the correlated flickering along the entire microrod. The x- and y-axes labels represent the time difference and the starting time of the corresponding row, respectively. (d) Scatter plot correlating the intensity of two domains (*I* vs. *II*, *I* vs. *III* and *II* vs. *III*) for each frame and corresponding PCC values. (e) Correlation coefficient matrix for each pair of pixels along the strip represented by a dotted white rectangle in (a), showing high correlation values along the entire strip.

To directly probe the extent of carrier migration, point excitation experiments were performed on MR-11. **Figure S7,** SI shows the PL image under point-excitation, with a narrow excitation spot (FWHM= ~240 nm) nearly centred on the microrod. Despite the localized excitation, we observed the emission extended well beyond the excitation domain. The emission profile reveals a significantly broader spread than the excitation profile. The intensity decays progressively along the length of the rod, on both sides of the excitation spot, with enhanced intensity at the edges. Following previous literature [20,30], the energy migration lengths are defined as the intensity spreads (L_1 and L_2) at ~20% of the maximum PL intensity. The calculated energy migration distance of ~ 700 nm in MR-11 provides direct evidence of migration of charge carriers.

In order to examine the nature of the spatial synchronicity under point-excitation, we further constructed PCC matrix along the length of MR. **Figure S7b** demonstrates the progressive decay in correlation from the point of excitation, along the length of MR-11. Specifically, the nanodomains closer to the excitation spot show a near perfect correlation while the farther domains exhibit a reduced synchronicity. This corroborates that the dip in synchronicity corresponds to the reduced charge carrier migration efficiency. We note that there is a notable increase in the emission intensity at the extreme distal ends of the rod. This behaviour supports that photon recycling (PR) and waveguide effects act in tandem to extend communication beyond the limits of carrier diffusion, ensuring that distal regions remain coupled to the excitation domain. The high refractive index of $CsPbBr_3$ supports waveguide-assisted propagation of emitted photons[40,41]. The guided photons undergo PR process, generate secondary excitons and extends the spatial extent of excitation energy migration. Previous reports have demonstrated that PR can sustain long-range communication even in geometrically confined systems, while that distal domains remain correlated (via PR) even when carrier diffusion alone is insufficient.[20,30]

Similar reports on the OHPs suggested that the carrier migration plays a vital role for synchronicity in a microcrystal[20], owing to the organic A-site cation in $MAPbBr_3$, softer lattice dynamics, long carrier lifetimes, high charge carrier mobility (~30 $cm^2\ V^{-1}\ s^{-1}$) and diffusion lengths exceeding 5–10 μm [42]. In contrast, the fully inorganic lattice of $CsPbBr_3$ offers greater thermal stability but relatively low carrier mobilities (1–10 $cm^2\ V^{-1}\ s^{-1}$) and diffusion lengths of ~2–3 μm due to stronger electron–phonon coupling and faster trap-assisted recombination[43]. These differences explain why organometallic halide perovskite microcrystals often exhibit more robust spatial synchrony over extended domains, while $CsPbBr_3$ shows strong correlation

only within shorter ranges and relies more heavily on waveguide-assisted PR to sustain long-range communication. These findings reinforce the universality of spatially correlated blinking in perovskite microstructures and extend previous observations in OHPs to all-inorganic $CsPbBr_3$ system.

While carrier diffusion and the waveguide effect offer a robust framework for understanding synchronous behaviour in MRs, these mechanisms alone cannot fully account for the behaviour of longer rods without addressing the vital role of transient traps. Prevailing theory ascribes the quenching of substantial subpopulation of photoexcited carriers over the entire crystal volume to "*special quenchers*" {metastable non-radiative (NR) traps}, which exhibit high quenching efficiency, surpassing the internal defects of the crystal by several order of magnitude. It has been hypothesized that *special quenchers* act like a donor-acceptor pair complexes. When the donor-acceptor species are in close proximity, the complex is changed in an active state capable of quenching large number of electrons and hole simultaneously, leading to extremely efficient nonradiative recombination.[17] It is emphasized that, NR traps are photogenerated, influenced by excitation conditions and the local environment around the crystals (vide infra).

To understand the nature and origin of such NR traps, we irradiate the MRs under 405 nm laser at different power densities. The measurements were started with minimum laser power with a gradual increase in the excitation power density to minimize the photo-degradation. **Figure S8,** SI depicts the PL intensity traces (left) and average intensity images (right) of MR-12. The PL trajectories of the MR-12 show a progressive increase in the emission fluctuations with increase in excitation power density. This behaviour reveals that a photo induced quenching mechanism is responsible for the high blinking amplitude, wherein the species responsible for quenching (NR traps) are dynamically generated or activated by the incident light flux rather than being inherent, stable defects[44]. Also, we note that with the increase in the power density and excitation energy, the cross-correlation matrix shows higher synchronicity. Similar types of behaviour were also noticed in the energy dependent study, where the PL fluctuation amplitude of MR-13 is higher in the 405 nm excitation compared to 473 and 488 nm (**Figure S9,** SI).

3.4 Environmental Dependence of Photoluminescence in All-Inorganic $CsPbBr_3$ Microcrystals

To comprehend the origins of metastable nature of the NR traps, we investigated the PL flickering dynamics of $CsPbBr_3$ MRs under sequential change of environmental conditions, which revealed a complex, reversible interplay between molecular adsorbates and transient nonradiative recombination centres. The PL trajectories of MR-5 shown in **Figure 4a** illustrate

that the $CsPbBr_3$ microcrystals are highly sensitive to the change in local environment. We have emphasized that the measurements were performed on the same MRs under different ambient conditions, as different MRs may have different flickering properties. We find that, under ambience (Air, ~50 % RH), MR-5 exhibits moderate PL intensity and continuous flickering, indicative of metastable trap states switching between active and passive states. Transitioning to dry argon leads to a sudden and nearly complete quenching of PL, while with introduction of moisture via argon (RH ~50%), a visible enhancement in the PL intensity and fluctuation was noticed. Despite argon being an inert gas (non-interacting), we believe that Ar somehow creates a large number of a different type of NR traps which are not the metastable traps responsible blinking phenomenon reported here. Since blinking is governed by few metastable traps, the existence of a large number of alternate NR centers may result in a massive drop in the PL intensity with no notable PL fluctuation. This proposed mechanism aligns with prior reports of abrupt PL suppression in perovskite microrods due to trap activation in inert atmospheres[45]. With the introduction of moisture via argon (RH ~50%), a visible enhancement in the PL intensity and fluctuation is noticed, owing to the formation of reversible transient traps.

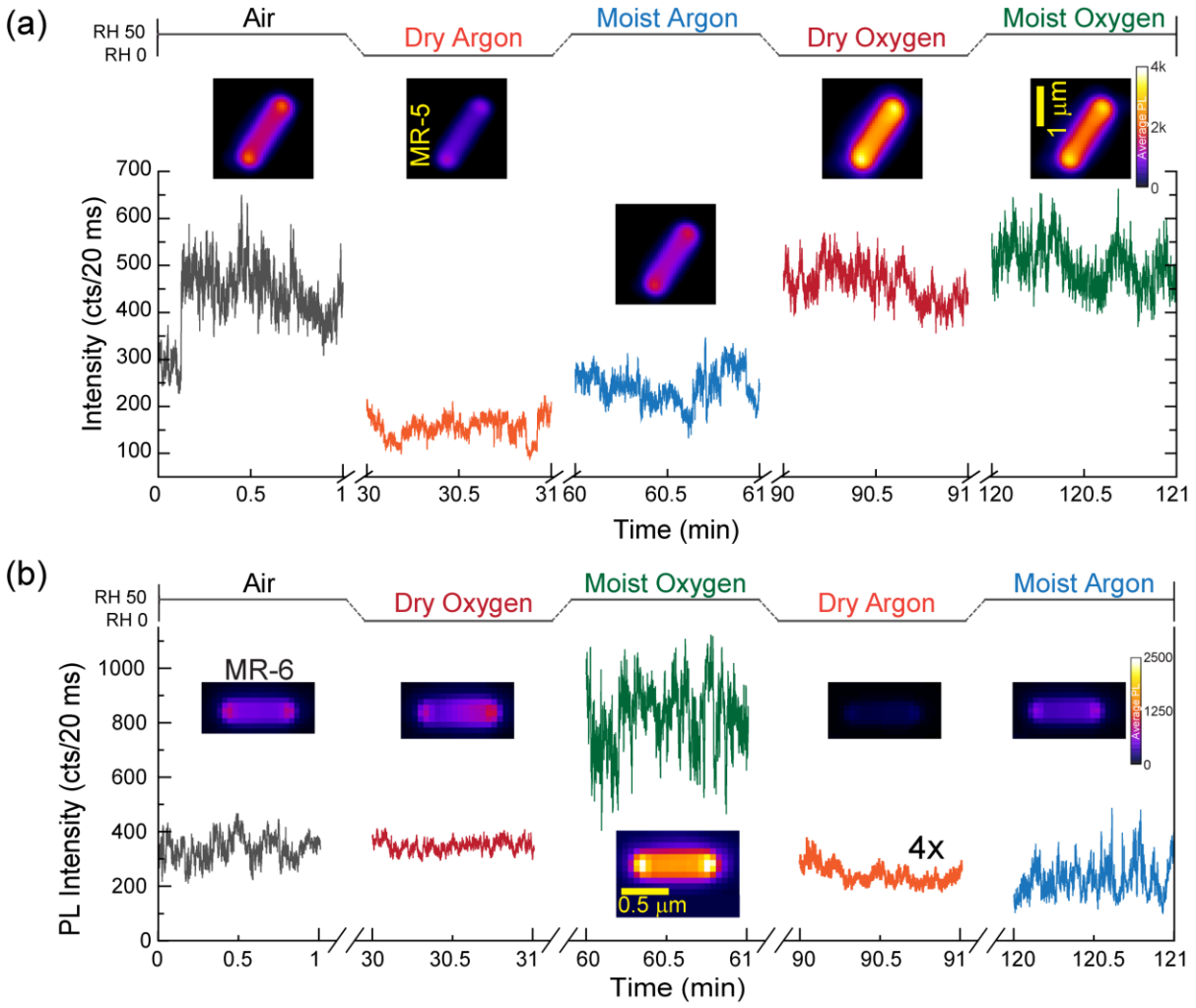

Figure 4. PL flickering variation of MRs under varying environmental conditions. (a) PL intensity trajectories of MR-5 under sequential exposure to different gas environments: ambient (RH 50%), dry argon (RH 0%), moist argon (RH 50%), dry oxygen (RH 0%), and moist oxygen (RH 50%). (b) PL intensity trajectories of MR-6 under reverse order of gas injection. The corresponding time averaged PL images are shown as inset.

Further, upon exposure of MR-5 to dry oxygen (RH ≈ 0%), the average PL intensity noticeably changes although the PL fluctuations are not so vigorous. The increase in the intensity under dry oxygen from moist argon can be a consequence of the depletion of NR traps formed under argon (dry/moist) environments. Again, the competing nature of O_2 as a passivating agent to the surface defects and inherent property to the formation or accumulation of less efficient nonradiative traps in the absence of moisture causes less flickering with a high intensity baseline. [22,26] Interestingly, the reintroduction of moisture via oxygen to the local environment of MR-5 results in dramatic PL recovery and the emergence of vigorous multistate flickering events. Moisture acts as a transient passivating agent, which can adsorb onto the surface defects such as halide vacancies (or unsaturated bonds), enables rapid switching of special traps between active and passive states. This behaviour is supported by studies showing

that water/oxygen molecules can reversibly passivate surface traps and enhance PL in $CsPbBr_3$ thin films[26].

We further recorded PL movies of MR-6 under an alternative environmental sequence, introducing oxygen prior to argon in order to examine the influence of gas injection order on the observed dynamics (**Figure 4b**). Irrespective of the gas injection sequence, a consistent pattern of intensity and fluctuation modulations was observed across all investigated environmental conditions, highlighting the dynamic and reversible nature of these non-radiative channels. We found similar observations in multiple other MRs; however, we found a few situations where the PL flickering of certain MRs were found in some cases where the MR deviates from the abovementioned trend. These anomalies are likely connected to the intrinsic properties of specific crystals or to defects present within them, though the underlying mechanisms remain unclear and warrant further investigation.

Thus, the PL properties of $CsPbBr_3$ microcrystals are governed by a dual mechanism: argon introduces highly efficient NR traps, which are large in number and reduces the overall PLQY, while moisture via oxygen enables dynamic, reversible passivation, leading to high quantum yield and spatially correlated flickering. However, oxygen induces very few of the special traps which enhance spatially correlated flickering/blinking. These insights are critical for optimizing perovskite-based optoelectronic devices, where environmental control can be leveraged to tune emission properties.

4. Conclusion

To conclude, our study demonstrates that all-inorganic $CsPbBr_3$ microrods, despite their reported emission stability, can exhibit pronounced multi-level photoluminescence fluctuations characterized by abrupt flickering events and spatially synchronous blinking across micrometer-scale domains. Correlation analyses reveal that the entire microrod behaves as if it is a single emissive entity, with blinking synchronicity sustained through a combination of carrier migration, photon recycling, and waveguide-assisted propagation. Importantly, the flickering dynamics are strongly modulated by excitation power, photon energy, and local atmospheric composition, underscoring the metastable and photoinduced nature of nonradiative traps that govern emission intermittency. These findings extend the universality of spatiotemporally correlated blinking beyond organometallic halide perovskites to fully inorganic systems, highlighting the crucial role of transient defects and environmental interactions in dictating the photophysical behaviour of perovskite microstructures, in general.

Declaration of competing interest

The authors declare no conflict of interest.

Acknowledgments

AC acknowledges SERB, Department of Science and Technology (DST), Govt. of India (Project code: RD/0118-DST0000062) for financial support to carry out this work. AC also appreciate MNRE (Govt. of India) aided NCPRE for partial financial support. Authors acknowledge CRNTS-SAIF and Central Facilities of IIT Bombay for their support with characterization. SP acknowledge IIT Bombay for Institute Post-doc fellowship. SS thanks Prime Minister's Research Fellowship, India for the PhD scholarship.

References

(1) Stranks, S. D.; Eperon, G. E.; Grancini, G.; Menelaou, C.; Alcocer, M. J. P.; Leijtens, T.; Herz, L. M.; Petrozza, A.; Snaith, H. J. Electron-Hole Diffusion Lengths Exceeding 1 Micrometer in an Organometal Trihalide Perovskite Absorber. *Science (1979)* 2013, *342* (6156), 341–344. https://doi.org/10.1126/science.1243982.

(2) Zhang, C.; Kuang, D.; Wu, W. A Review of Diverse Halide Perovskite Morphologies for Efficient Optoelectronic Applications. *Small Methods* 2020, *4* (2). https://doi.org/10.1002/smtd.201900662.

(3) Chen, J.; Zhou, S.; Jin, S.; Li, H.; Zhai, T. Crystal Organometal Halide Perovskites with Promising Optoelectronic Applications. *J Mater Chem C Mater* 2016, *4* (1), 11–27. https://doi.org/10.1039/C5TC03417E.

(4) Fu, Y.; Zhu, H.; Chen, J.; Hautzinger, M. P.; Zhu, X.-Y.; Jin, S. Metal Halide Perovskite Nanostructures for Optoelectronic Applications and the Study of Physical Properties. *Nat Rev Mater* 2019, *4* (3), 169–188. https://doi.org/10.1038/s41578-019-0080-9.

(5) Kovalenko, M. V.; Protesescu, L.; Bodnarchuk, M. I. Properties and Potential Optoelectronic Applications of Lead Halide Perovskite Nanocrystals. *Science (1979)* 2017, *358* (6364), 745–750. https://doi.org/10.1126/science.aam7093.

(6) Huang, J.; Yuan, Y.; Shao, Y.; Yan, Y. Understanding the Physical Properties of Hybrid Perovskites for Photovoltaic Applications. *Nat Rev Mater* 2017, *2* (7), 17042. https://doi.org/10.1038/natrevmats.2017.42.

(7) Halder, A.; Pathoor, N.; Chowdhury, A.; Sarkar, S. K. Photoluminescence Flickering of Micron-Sized Crystals of Methylammonium Lead Bromide: Effect of Ambience and Light Exposure. *The Journal of Physical Chemistry C* 2018, *122* (27), 15133–15139. https://doi.org/10.1021/acs.jpcc.8b03862.

(8) Jiang, Y.; Yuan, J.; Ni, Y.; Yang, J.; Wang, Y.; Jiu, T.; Yuan, M.; Chen, J. Reduced-Dimensional α-CsPbX3 Perovskites for Efficient and Stable Photovoltaics. *Joule* 2018, *2* (7), 1356–1368. https://doi.org/10.1016/j.joule.2018.05.004.

(9) Behera, T.; Pathoor, N.; Phadnis, C.; Buragohain, S.; Chowdhury, A. Spatially Correlated Photoluminescence Blinking and Flickering of Hybrid-Halide Perovskite Micro-Rods. *J Lumin* 2020, *223*, 117202. https://doi.org/10.1016/j.jlumin.2020.117202.

(10) Swarnkar, A.; Chulliyil, R.; Ravi, V. K.; Irfanullah, M.; Chowdhury, A.; Nag, A. Colloidal CsPbBr 3 Perovskite Nanocrystals: Luminescence beyond Traditional Quantum Dots. *Angewandte Chemie International Edition* 2015, *54* (51), 15424–15428. https://doi.org/10.1002/anie.201508276.

(11) Dickson, R. M.; Cubitt, A. B.; Tsien, R. Y.; Moerner, W. E. On/off Blinking and Switching Behaviour of Single Molecules of Green Fluorescent Protein. *Nature* 1997, *388* (6640), 355–358. https://doi.org/10.1038/41048.

(12) Tachikawa, T.; Karimata, I.; Kobori, Y. Surface Charge Trapping in Organolead Halide Perovskites Explored by Single-Particle Photoluminescence Imaging. *J Phys Chem Lett* 2015, *6* (16), 3195–3201. https://doi.org/10.1021/acs.jpclett.5b01566.

(13) Efros, A. L.; Nesbitt, D. J. Origin and Control of Blinking in Quantum Dots. *Nat Nanotechnol* 2016, *11* (8), 661–671. https://doi.org/10.1038/nnano.2016.140.

(14) Glennon, J. J.; Tang, R.; Buhro, W. E.; Loomis, R. A. Synchronous Photoluminescence Intermittency (Blinking) along Whole Semiconductor Quantum Wires. *Nano Lett* 2007, *7* (11), 3290–3295. https://doi.org/10.1021/nl0714583.

(15) Protasenko, V. V.; Hull, K. L.; Kuno, M. Disorder-Induced Optical Heterogeneity in Single CdSe Nanowires. *Advanced Materials* 2005, *17* (24), 2942–2949. https://doi.org/10.1002/adma.200501660.

(16) Si, J.; Volkán-Kacsó, S.; Eltom, A.; Morozov, Y.; McDonald, M. P.; Kuno, M.; Jankó, B. Heterogeneous Fluorescence Intermittency in Single Layer Reduced Graphene Oxide. *Nano Lett* 2015, *15* (7), 4317–4321. https://doi.org/10.1021/acs.nanolett.5b00191.

(17) Merdasa, A.; Tian, Y.; Camacho, R.; Dobrovolsky, A.; Debroye, E.; Unger, E. L.; Hofkens, J.; Sundström, V.; Scheblykin, I. G. "Supertrap" at Work: Extremely Efficient Nonradiative Recombination Channels in MAPbI 3 Perovskites Revealed by Luminescence Super-Resolution Imaging and Spectroscopy. *ACS Nano* 2017, *11* (6), 5391–5404. https://doi.org/10.1021/acsnano.6b07407.

(18) Pathoor, N.; Chowdhury, A. Spatially Correlated Blinking of Perovskite Micro-Crystals: Deciphering Effective Modes of Communication between Distal Photoexcited Carriers. *ACS Photonics* 2023, *10* (1), 49–57. https://doi.org/10.1021/acsphotonics.2c00884.

(19) Yuan, H.; Debroye, E.; Caliandro, G.; Janssen, K. P. F.; van Loon, J.; Kirschhock, C. E. A.; Martens, J. A.; Hofkens, J.; Roeffaers, M. B. J. Photoluminescence Blinking of Single-Crystal Methylammonium Lead Iodide Perovskite Nanorods Induced by Surface Traps. *ACS Omega* 2016, *1* (1), 148–159. https://doi.org/10.1021/acsomega.6b00107.

(20) Chen, R.; Xia, B.; Zhou, W.; Zhang, G.; Qin, C.; Hu, J.; Scheblykin, I. G.; Xiao, L. Environment-Dependent Metastable Nonradiative Recombination Centers in Perovskites Revealed by Photoluminescence Blinking. *Adv Photonics Res* 2022, *3* (1). https://doi.org/10.1002/adpr.202100271.

(21) Yuan, H.; Debroye, E.; Bladt, E.; Lu, G.; Keshavarz, M.; Janssen, K. P. F.; Roeffaers, M. B. J.; Bals, S.; Sargent, E. H.; Hofkens, J. Imaging Heterogeneously Distributed Photo-Active Traps in Perovskite Single Crystals. *Advanced Materials* 2018, *30* (13). https://doi.org/10.1002/adma.201705494.

(22) Behera, T.; Chowdhury, A. Unravelling the Role of Metastable Quenchers in Spatially (Un)Correlated Blinking of Perovskite Micro-Rods. November 20, 2025. https://doi.org/10.26434/chemrxiv-2025-cs8t7.

(23) Hong, D.; Zhang, Y.; Pan, S.; Liu, H.; Mao, W.; Lu, Z.; Tian, Y. Moisture-Dependent Blinking of Individual CsPbBr 3 Nanocrystals Revealed by Single-Particle Spectroscopy. *J Phys Chem Lett* 2022, *13* (46), 10751–10758. https://doi.org/10.1021/acs.jpclett.2c03159.

(24) Anni, M.; Cretì, A.; Zhang, Y.; De Giorgi, M. L.; Lomascolo, M. Investigation of the Role of the Environment on the Photoluminescence and the Exciton Relaxation of $CsPbBr_3$ Nanocrystals Thin Films. *Applied Sciences* 2020, *10* (6), 2148. https://doi.org/10.3390/app10062148.

(25) Pathoor, N.; Halder, A.; Mukherjee, A.; Mahato, J.; Sarkar, S. K.; Chowdhury, A. Fluorescence Blinking Beyond Nanoconfinement: Spatially Synchronous Intermittency of Entire Perovskite Microcrystals. *Angewandte Chemie International Edition* 2018, *57* (36), 11603–11607. https://doi.org/10.1002/anie.201804852.

(26) Feng, S.; Qin, Q.; Han, X.; Zhang, C.; Wang, X.; Yu, T.; Xiao, M. Universal Existence of Localized Single-Photon Emitters in the Perovskite Film of All-Inorganic CsPbBr 3 Microcrystals. *Advanced Materials* 2022, *34* (1). https://doi.org/10.1002/adma.202106278.

(27) Jiang, L.; Liu, R.; Su, R.; Yu, Y.; Xu, H.; Wei, Y.; Zhou, Z.-K.; Wang, X. Continuous Wave Pumped Single-Mode Nanolasers in Inorganic Perovskites with Robust Stability and High Quantum Yield. *Nanoscale* 2018, *10* (28), 13565–13571. https://doi.org/10.1039/C8NR03830A.

(28) Behera, T.; Pathoor, N.; Mukherjee, R.; Chowdhury, A. Deciphering Modes of Long-Range Energy Transfer in Perovskite Crystals Using Confocal Excitation and Wide-Field Fluorescence Spectral Imaging. *Methods Appl Fluoresc* 2022, *10* (4), 044013. https://doi.org/10.1088/2050-6120/ac8f85.

(29) Mukherjee, A.; Roy, M.; Pathoor, N.; Aslam, M.; Chowdhury, A. Influence of Atmospheric Constituents on Spectral Instability and Defect-Mediated Carrier Recombination in Hybrid Perovskite Nanoplatelets. *The Journal of Physical Chemistry C* 2021, *125* (31), 17133–17143. https://doi.org/10.1021/acs.jpcc.1c02207.

(30) Schneider, C. A.; Rasband, W. S.; Eliceiri, K. W. NIH Image to ImageJ: 25 Years of Image Analysis. *Nat Methods* 2012, *9* (7), 671–675.

(31) Rodová, M.; Brožek, J.; Knížek, K.; Nitsch, K. Phase Transitions in Ternary Caesium Lead Bromide. *J Therm Anal Calorim* 2003, *71* (2), 667–673. https://doi.org/10.1023/A:1022836800820.

(32) Duong, T.-T.; Tran, P.-N.; Van, T.-P.; Nguyen, D.-H.; Tran, V.-D. A Dense, Pinholes-Free Pure Cubic Phase $CsPbBr_3$ Nanocrystals Film for High-Performance Photodetector. *Electronic Materials Letters* 2024, *20* (2), 217–223. https://doi.org/10.1007/s13391-023-00448-x.

(33) Xu, F.; Li, Y.; Yuan, B.; Zhang, Y.; Wei, H.; Wu, Y.; Cao, B. Large-Area $CsPbBr_3$ Perovskite Films Grown with Effective One-Step RF-Magnetron Sputtering. *J Appl Phys* 2021, *129* (24). https://doi.org/10.1063/5.0050810.

(34) Tian, W.; Cui, R.; Leng, J.; Liu, J.; Li, Y.; Zhao, C.; Zhang, J.; Deng, W.; Lian, T.; Jin, S. Limiting Perovskite Solar Cell Performance by Heterogeneous Carrier Extraction. *Angewandte Chemie International Edition* 2016, *55* (42), 13067–13071. https://doi.org/10.1002/anie.201606574.

(35) Dou, L.; Wong, A. B.; Yu, Y.; Lai, M.; Kornienko, N.; Eaton, S. W.; Fu, A.; Bischak, C. G.; Ma, J.; Ding, T.; Ginsberg, N. S.; Wang, L.-W.; Alivisatos, A. P.; Yang, P. Atomically Thin Two-Dimensional Organic-Inorganic Hybrid Perovskites. *Science (1979)* 2015, *349* (6255), 1518–1521. https://doi.org/10.1126/science.aac7660.

(36) Halder, A.; Chulliyil, R.; Subbiah, A. S.; Khan, T.; Chattoraj, S.; Chowdhury, A.; Sarkar, S. K. Pseudohalide (SCN –)-Doped MAPbI 3 Perovskites: A Few Surprises. *J Phys Chem Lett* 2015, *6* (17), 3483–3489. https://doi.org/10.1021/acs.jpclett.5b01327.

(37) Lee, S. F.; Osborne, M. A. Brightening, Blinking, Bluing and Bleaching in the Life of a Quantum Dot: Friend or Foe? *ChemPhysChem* 2009, *10* (13), 2174–2191. https://doi.org/10.1002/cphc.200900200.

(38) Kiligaridis, A.; Merdasa, A.; Rehermann, C.; Unger, E. L.; Scheblykin, I. G. Excitation Wavelength Dependence of Photoluminescence Flickering in Degraded MAPbI3 Perovskite and Its Connection to Lead Iodide Formation. *J Lumin* 2020, *222*, 117129. https://doi.org/10.1016/j.jlumin.2020.117129.

(39) Eaton, S. W.; Lai, M.; Gibson, N. A.; Wong, A. B.; Dou, L.; Ma, J.; Wang, L.-W.; Leone, S. R.; Yang, P. Lasing in Robust Cesium Lead Halide Perovskite Nanowires. *Proceedings of the National Academy of Sciences* 2016, *113* (8), 1993–1998. https://doi.org/10.1073/pnas.1600789113.

(40) Ahmad Kamal, A. S.; Lin, C.-C.; Wang, Z.; Xing, D.; Lee, Y.-C.; Chen, M.-H.; Ho, Y.-L.; Chen, C.-W.; Delaunay, J.-J. $CsPbBr_3$ Nanocrystals Plasmonic Distributed Bragg Reflector Waveguide Laser. *Appl Phys Lett* 2023, *122* (7). https://doi.org/10.1063/5.0128232.

(41) Ščajev, P.; Miasojedovas, S.; Juršėnas, S. A Carrier Density Dependent Diffusion Coefficient, Recombination Rate and Diffusion Length in MAPbI 3 and MAPbBr 3 Crystals Measured under One- and Two-Photon Excitations. *J Mater Chem C Mater* 2020, *8* (30), 10290–10301. https://doi.org/10.1039/D0TC02283G.

(42) Ullah, S.; Wang, J.; Yang, P.; Liu, L.; Yang, S.-E.; Xia, T.; Guo, H.; Chen, Y. All-Inorganic CsPbBr 3 Perovskite: A Promising Choice for Photovoltaics. *Mater Adv* 2021, *2* (2), 646–683. https://doi.org/10.1039/D0MA00866D.

(43) Pathoor, N.; Mukherjee, A.; Chowdhury, A. Investigating Spatiotemporal Correlation of Multi-State Photoluminescence Intermittency in Organo-Lead Bromide Microcrystal Films. *The Journal of Physical Chemistry C* 2022, *126* (13), 5991–5999. https://doi.org/10.1021/acs.jpcc.1c10760.

(44) Ye, X.; Li, C.; Jiang, J.; Zheng, X.; Han, Q.; Lin, Q.; Liu, Y.; Tao, X. Morphology Dependent Light-Induced Photoluminescence Enhancement of CsPbBr 3 Microcrystals. *Chemical Communications* 2023, *59* (23), 3403–3406. https://doi.org/10.1039/D2CC06545B.